Computers and Geotechnics 170 (2024) 106266

Contents lists available at ScienceDirect

Computers and Geotechnics

journal homepage: www.elsevier.com/locate/compgeo

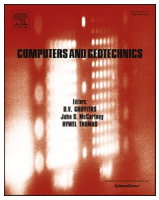

Research Paper

# An uncoupled approach for estimating seismic-induced pore water pressures in liquefiable sandy soils

Gabriele Boccieri [a,*], Domenico Gaudio [b], Riccardo Conti [c]

[a] Università di Roma Niccolò Cusano, Via Don Carlo Gnocchi 3, 00166 Rome, Italy
[b] Dept. of Geotechnical and Structural Engineering, Sapienza Università di Roma, via Eudossiana 18, 00184 Rome, Italy
[c] Dept. of Civil Engineering and Computer Science Engineering, Università degli Studi di Roma Tor Vergata, Via del Politecnico, 1, 00133 Rome, Italy

ARTICLE INFO

*Keywords:*
Excess pore water pressure
Liquefaction
Number of equivalent cycles
Uncoupled approach
Numerical analyses
Earthquake

ABSTRACT

Proper evaluation of seismic-induced excess pore water pressures in saturated sandy soils is still an open issue, which can be tackled with fully coupled to uncoupled approaches. The former are more accurate but computationally onerous, while the latter require seismic demand and pore pressure build-up to be computed in two successive steps, typically employing simple constitutive assumptions.

Starting from the work by Seed *et al.* (1975), this paper presents a novel uncoupled procedure to compute excess water pressures developing in a 1D soil column under partially drained conditions, when subjected to horizontal seismic excitations. Fundamental modifications are introduced to account for: non-uniform distribution of equivalent loading cycles; soil stiffness degradation; and modification of the frequency content of ground motion due to pore pressure build-up.

The approach was implemented in Matlab via the Finite Difference Method and validated against both fully-coupled Finite Element analyses and one centrifuge test. An extensive parametric study was also performed for a two-layer soil column, by varying the thickness and hydraulic conductivity of the shallow layer, as well as the seismic input. The good agreement with both numerical and experimental data demonstrates that key features of liquefaction are well-captured by the proposed uncoupled approach.

## 1. Introduction

The seismic-induced build-up of pore water pressures in saturated sandy soils, possibly leading to liquefaction, is primarily due to the volumetric-distortional coupling peculiar of soil mechanical behaviour. The occurrence of this phenomenon in the field depends on a number of factors, including: (i) the intensity, frequency content and duration of the input earthquake (Kramer *et al.*, 2016); (ii) the initial depth of the water table within the soil deposit, as well as the depth and thickness of the liquefiable layer (Minaka *et al.*, 2021); (iii) the hydraulic conductivity of the liquefiable and of the adjacent soil layers (Ni *et al.*, 2021). Among these, the drainage condition imposed by the adjacent layers affects the evolution of pore water pressures during both the strong-motion phase, which does not always occur as an undrained process (Adamidis and Anastasopoulos, 2022), and the subsequent consolidation phase, when seepage-induced liquefaction can arise in the shallowest layers (Boulanger and Idriss, 2014; Cubrinovski *et al.*, 2019).

All methods for assessing the liquefaction potential of a given soil deposit are developed under the simplifying assumption of one-dimensional free-field shear wave propagation, following either coupled or uncoupled approaches (Cubrinovski *et al.*, 2019; Rios *et al.*, 2022; Cubrinovski and Ntritsos, 2023; Ntritsos and Cubrinovski, 2024)

Coupled approaches are based on time-domain effective stress analyses, where soil behaviour is described through advanced constitutive models and the evolution of pore water pressures stems from rigorous hydro-mechanical coupling or semi-empirical pore pressure generation models (Ramirez *et al.*, 2018; Tropeano *et al.*, 2019). Although providing accurate results, these approaches are rarely used in the engineering practice since they are time-consuming and rely on parameters not easy to calibrate.

Uncoupled approaches are typically used in the form of simplified stress-based methods, where the safety factor against liquefaction is defined as the ratio between the soil liquefaction resistance and the seismic demand, the latter being computed through either total-stress Seismic Site Response Analyses (SSRA) or simplified empirical equations. These methods rely on the assumption of fully undrained

* Corresponding author.
*E-mail addresses:* gabriele.boccieri@unicusano.it (G. Boccieri), domenico.gaudio@uniroma1.it (D. Gaudio), riccardo.conti@uniroma2.it (R. Conti).

https://doi.org/10.1016/j.compgeo.2024.106266
Received 13 January 2024; Received in revised form 3 March 2024; Accepted 22 March 2024

conditions (Adamidis and Anastasopoulos, 2022), thus neglecting any hydraulic interaction between different layers within the soil deposit (Sinha *et al.*, 2024), and their predictions are often inconsistent with field observations (Cubrinovski *et al.*, 2019). Moreover, they do not provide any information on the amount of excess pore water pressures generated when liquefaction is not fully attained, which is a relevant information when assessing the liquefaction potential through *ad-hoc* integral damage parameters (Chiaradonna *et al.*, 2020). Indeed, a substantial drop in the soil shear strength and stiffness of shallow layers can occur during seismic shaking – due to the reduction of effective stresses – even in the case when full liquefaction is not triggered (Chiaradonna and Flora, 2020).

Still following a stress-based uncoupled framework, a more refined approach was proposed by Seed *et al.* (1975), in which the excess pore water pressures arising in a liquefiable stratum are computed under general, partially drained conditions. Starting from their seminal work, this paper proposes a new uncoupled approach for the computation of excess pore water pressures induced in a one-dimensional soil column by a given seismic excitation. Fundamental modifications are introduced to account for: (i) a non-uniform distribution of equivalent loading cycles throughout the earthquake duration; (ii) the soil stiffness degradation and (iii) the modification of the frequency content of ground motion, both due to pore water pressures build-up and to the resulting decrease of effective stresses. Such new assumptions aim at achieving a simple but physically-sound solution, considering aspects of the liquefaction phenomenon that were neglected by Seed *et al.* (1975) and providing a better representation of both timing, evolution, and dissipation of seismic-induced pore water pressures within a given soil deposit.

A straightforward implementation of the proposed procedure is presented, by solving the governing equations through the Finite Difference Method (FDM). Finally, the method is validated against the results of coupled Finite Element (FE) analyses and experimental centrifuge tests (Özcebe *et al.*, 2021).

## 2. Proposed method

As in Seed *et al.* (1975), the proposed method decomposes the assessment of earthquake-induced pore water pressures into two successive steps:

1. the computation of earthquake-induced shear stresses, $\tau(t)$, at each depth within the soil column (seismic demand), through a 1D total-stress SSRA;
2. the computation of excess pore water pressures through the solution of the modified 1D consolidation equation (Terzaghi, 1923), where a source term is added to include pore-pressure generation due to earthquake loading ("modified 1D generation-diffusion model" in the following).

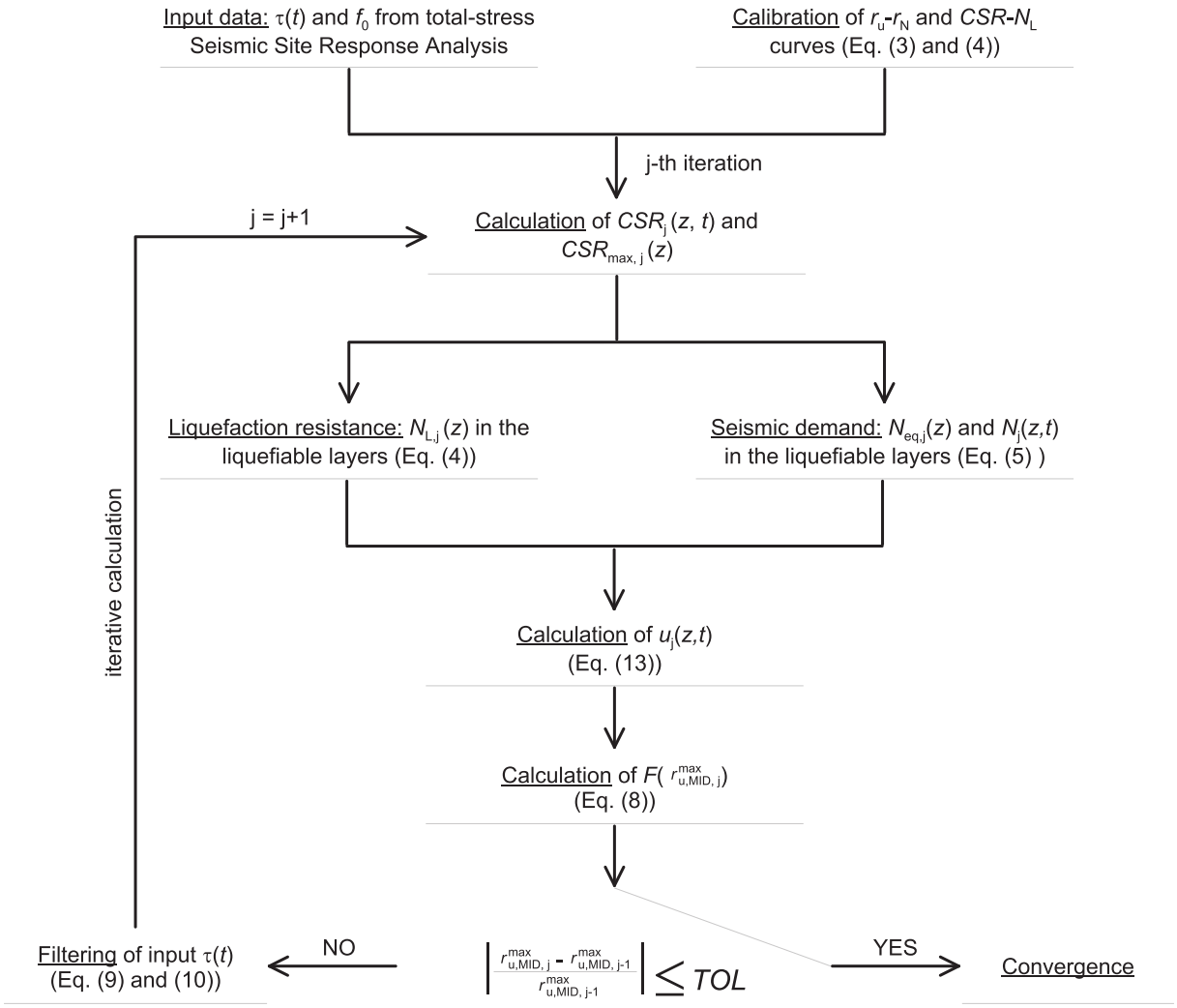


**Fig. 1.** Flowchart of the proposed method.

Fig. 1 shows a flowchart of the proposed method, outlining the required input parameters and the algorithm implemented to solve the modified 1D generation-diffusion model. Specifically, the latter is solved iteratively to easily account for the effect of generated pore pressures on the applied seismic demand. All steps are detailed in the following sections.

### 2.1. 1D seismic site response analysis

A nonlinear 1D total-stress SSRA is carried out to compute the time history of shear stresses at each depth within the stratified soil column, $\tau(t)$, representing the seismic demand for the successive steps (Fig. 2a and b). As a further outcome, the analysis provides the mobilised fundamental frequency of the soil deposit, $f_0$, indicating the frequency range where amplification effects are more pronounced. As shown in Fig. 2c, the latter can be computed from the surface-to-bedrock frequency-dependent transfer function.

In this work, the Modified Hardin and Drnevich (MHD) model proposed by Conti *et al.* (2020) was used, including both nonlinearity and strength in the constitutive equations. The model requires only six parameters: the small strain shear modulus, $G_0$; the soil shear strength, $\tau_{lim}$; $a$ and $b$, controlling the shear modulus decay curve, $G/G_0(\gamma)$; and $c$ and $d$, which govern the damping curve, $D(\gamma)$. Both $G_0$ and $\tau_{lim}$ depend on the mean effective stress, $p'$, while the remaining parameters depend solely on intrinsic soil properties.

### 2.2. Modified 1D generation-diffusion model

Earthquake-induced pore water pressures within a liquefiable soil layer are computed by solving the modified consolidation equation (Seed *et al.*, 1975):

$$\frac{\partial u}{\partial t} = c_v \frac{\partial^2 u}{\partial z^2} + \frac{\partial u_g}{\partial t} \tag{1}$$

where $c_v = k \bullet E'_{oed}/\gamma_w$ is the consolidation coefficient, $k$ is the hydraulic conductivity, $E'_{oed}$ is the oedometric modulus, and $\gamma_w = 9.81$ kN/m$^3$ is the water unit weight, while $\partial u_g/\partial t$ is a source term representing the rate of pore water pressure build-up occurring in fully undrained conditions, which depends on soil liquefaction resistance and seismic-induced shear stresses, both conventionally expressed in terms of equivalent cyclic loading.

Despite its very simplicity, Eq. (1) provides a clear picture of how pore pressures generate under partially drained conditions, including the extreme cases of fully undrained and drained conditions, in a comprehensive framework. Indeed, when the dissipative term, $c_v \bullet \partial^2 u/\partial z^2$, is small compared to the source term, $\partial u_g/\partial t$, then the excess pore pressures are similar to those developed in undrained conditions ($u \approx u_g$). On the contrary, when the two terms on the right-hand side attain almost the same absolute value, but opposite sign (*i.e.*, $c_v \bullet \partial^2 u/\partial z^2 \approx -\partial u_g/\partial t$), then $\partial u/\partial t \approx 0$, which represents fully drained conditions. Finally, when $\partial u_g/\partial t$ is relatively small or null (no driving input, as in the post-earthquake stage), the problem is ruled by 1D consolidation and excess pore water pressures gradually dissipate within the soil deposit.

To compute the source term, $\partial u_g/\partial t$, the irregular shear stress time history from SSRA, $\tau(t)$, is reduced to an equivalent cyclic loading, characterised by a constant amplitude $\tau_{eq} = 0.65 \cdot \tau_{max}$, a number of cycles $N_{eq}$, and a loading duration $T_d$ (Seed and Idriss, 1971). Accordingly, $\partial u_g/\partial t$ can be rewritten as:

$$\frac{\partial u_g}{\partial t} = \frac{\sigma'_{v0}}{N_L} \bullet \frac{dr_u}{dr_N} \bullet \frac{dN}{dt} \tag{2}$$

where $\sigma'_{v0}$ is the initial vertical effective stress; $N_L$ is the number of cycles needed to trigger liquefaction; $N$ is the n$^{th}$ cycle of loading; $r_u = u_g/\sigma'_{v0}$ is the excess pore pressure ratio; and $r_N = N/N_L$ is the cyclic ratio.

As detailed in the following, undrained cyclic laboratory results are used to evaluate both the $r_u$-$r_N$ curve, from which the derivative $dr_u/dr_N$ is obtained, and $N_L$. Moreover, a standard cumulative damage assumption is adopted to convert the irregular time history $\tau(t)$ into an equivalent number of uniform stress cycles, $N(t)$, from which the derivative $dN/dt$ is obtained.

#### 2.2.1. Excess pore water pressures relation and cyclic resistance curve

The $r_u$-$r_N$ function provides information on the accumulation of excess pore water pressures during undrained cyclic loading. As in Khashila *et al.* (2018), the following expression was considered in this work:

$$r_u = \chi \bullet r_N^{\theta} \tag{3}$$

where the two parameters $\chi$ and $\theta$ can be determined from cyclic laboratory test results.

The cyclic resistance curve $CSR$-$N_L$ provides the number of cycles to liquefaction, $N_L$, for a given value of the cyclic stress ratio $CSR = \tau_{eq}/\sigma'_{v0}$. As in Park *et al.* (2015) and Chiaradonna *et al.* (2018), the following power function was adopted:

$$CSR = CSR_t + \beta \bullet N_L^{-\eta} \tag{4}$$

where parameters $\beta$ and $\eta$ define the intercept and slope of the curve in a

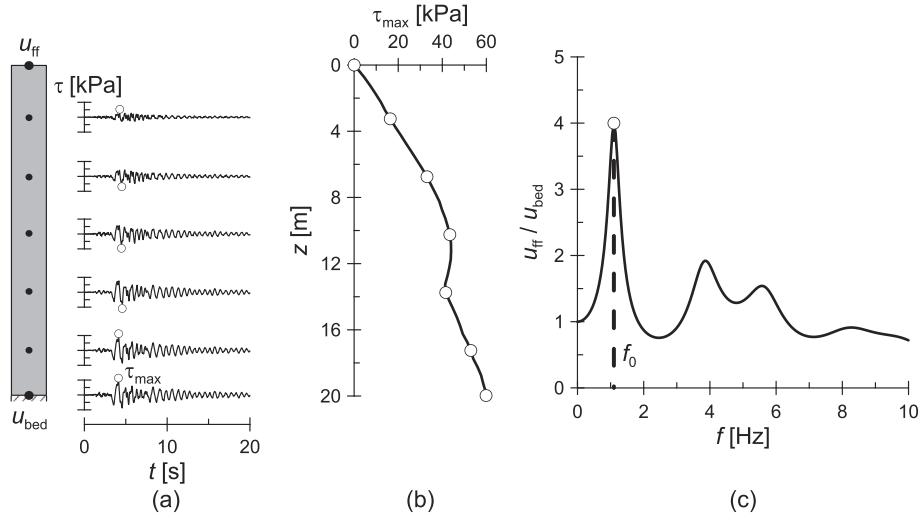


**Fig. 2.** Output from 1D total-stress SSRA: (a) shear stress time histories at different depths; (b) maximum shear stress profile; (c) soil column amplification.

semi-logarithmic plane, while $CSR_t$ is a threshold value below which excess pore water pressures are not generated when the soil sample is cyclically loaded in undrained conditions.

### 2.2.2. Equivalent cyclic loading

As in Seed *et al.* (1975), the equivalent number of cycles, $N_{eq}$, was computed under the hypothesis of linear damage accumulation (Miner, 1945). Specifically, considering the curve $CSR$–$N_L$ given by Eq. (4) as the locus of same damage level (*i.e.*, initial liquefaction), $N_{eq}$ was computed using the peak-counting method, where the number of largest peaks between adjacent zero-crossings is considered (Hancock and Bommer, 2005). Accordingly:

$$N_{eq} = \frac{1}{2}\sum_{i=1}^{N_{hc}} X_i \tag{5}$$

with

$$X_i = \begin{cases} \left(\dfrac{|CSR_{0.65}| - CSR_t}{|CSR_i| - CSR_t}\right)^{-1/\eta} & if\ |CSR_i| > CSR_t \\ 0 & if\ |CSR_i| \le CSR_t \end{cases} \tag{6}$$

where $N_{hc}$ is the total number of half cycles in the time history $\tau(t)$, $\tau_i$ is the corresponding amplitude, $CSR_{0.65} = \tau_{eq}/\sigma'_{v0}$ and $CSR_i = \tau_i/\sigma'_{v0}$. It is worth mentioning here that the coefficient 0.65, which is customarily adopted to compute $\tau_{eq}$, does not affect the results discussed herein. In fact, since it appears both in the numerator and the denominator of $\partial u_g/\partial t$, as it can be easily verified by comparing Eq. (2) with Eqs. (4)–(6), this coefficient drops out from the solution of the modified consolidation equation.

Eqs. (5) and (6) were also used to compute the cumulative distribution of the number of cycles $N(t)$, with $N_{hc}$ being, in this case, the number of half cycles up to time $t$. This procedure overcomes the assumption of uniform distribution of $N_{eq}$ along the loading duration $T_d$, as initially proposed by Seed *et al.* (1975), providing a more realistic description of the energy content of the applied irregular loading and, therefore, of the induced pore water pressures build-up. Accordingly, the derivative $dN/dt$ in Eq. (2) is no longer constant and must be computed numerically.

### 2.2.3. Signal filtering and check for convergence

As observed by many Authors (Bouckovalas *et al.*, 2016; Özener *et al.*, 2020; Millen *et al.*, 2021), pore water pressure build-up within liquefiable layers has two main effects: it induces soil stiffness degradation, thus reducing the fundamental site frequency compared with the non-liquefied soil column, and increases soil damping. As a result, excess pore pressures affect wave propagation, leading to an overall de-amplification of the high frequency components of ground motion. From a mechanical point of view, the occurrence of liquefaction in a given soil layer reduces the amount of inertia forces and shear stresses induced by travelling waves in the overlaying layers and then mitigates the further generation of excess pore-pressures (Cubrinovski *et al.*, 2019).

Liquefaction-induced filtering of earthquake motion cannot be captured by standard uncoupled approaches, where the seismic demand is computed based on total-stress SSRAs. A major outcome of this inherent limitation is a systematic overprediction of both $N_{eq}$ and excess pore water pressures when significant values of $r_u$ develop within the soil column (Rios *et al.*, 2022).

To overcome this drawback, a simple iterative procedure was implemented in the present study by exploiting the Stockwell transform (S-transform) for the time-frequency decomposition of a signal $h(t)$ (Stockwell *et al.*, 1996):

$$S(t,f) = \int_{-\infty}^{+\infty} h(\tau) e^{-\frac{(t-\tau)^2 f^2}{2}} e^{-i2\pi f t} d\tau \tag{7}$$

Taking advantage of its invertibility, the S-transform allows to apply different frequency filters in different time windows, thus modifying the frequency content of a given signal along its duration.

The key idea was to use the excess pore pressures computed at the $j^{th}$ iteration to identify when and how to filter the shear stresses $\tau(t)$, *i.e.*, the seismic demand, to be applied at the $(j+1)^{th}$ iteration. Specifically, the time history of the pore pressure ratio computed at the centre of the liquefiable layer, $r_{u,MID}(t)$, was used as a convenient indicator of the overall soil column behaviour at the $j^{th}$ iteration.

Based on theoretical and practical considerations (Özener *et al.*, 2020; Millen *et al.*, 2021), it was assumed that pore pressure ratios $r_{u,MID} < 0.2$ do not affect earthquake-induced shear stresses. For larger values of $r_{u,MID}$, the high-frequency components of shear stresses $\tau(t)$ are reduced by a factor $F\left(r^{max}_{u,MID}\right)$, where $r^{max}_{u,MID} = \max\left(r_{u,MID}\right)$:

$$F\left(r^{max}_{u,MID}\right) = 1 - a_1\left(r^{max}_{u,MID} - 0.2\right)^{a_2} \tag{8}$$

where coefficients $a_1 = 0.65$ and $a_2 = 0.25$ were calibrated based on the results of eleven advanced fully coupled FE analyses (Fig. 3), using a trial-and-error procedure to seek the value of $F$ providing the best match between the proposed approach and the reference FE analyses in terms of computed excess pore pressures. The filter $F$ was applied to frequencies $f \ge 0.8 \cdot f_0$, where $f_0$ is the fundamental frequency of the soil deposit, as inferred from total stress SSRA.

Based on the above procedure, and being $S(t,f)$ the S-transform of the shear stress $\tau(t)$ at a given depth, the S-transform of the filtered shear stress, $\widehat{S}(t,f)$, was computed as:

$$\widehat{S}(t,f) = \widehat{F}(t,f) \bullet S(t,f) \tag{9}$$

where:

$$\widehat{F}(t,f) = \begin{cases} 1 & (t < \widehat{t}) \text{ or } (t \ge \widehat{t}, f < 0.8 f_0) \\ F\left(r^{max}_{u,MID}\right) & (t \ge \widehat{t}, f \ge 0.8 f_0) \end{cases} \tag{10}$$

and $\widehat{t}$ is the first time instant when $r_{u,MID}$ reaches 0.2. An example is given in Fig. 4, showing: (a) the time history of the shear stress before and after filtering, together with $r_{u,MID}(t)$; (b) the S-transform of the original $\tau(t)$; and (c) the S-transform $\widehat{S}(t,f)$ of the filtered shear stress (units: kPa), computed for $\widehat{t} = 3.0$ s and $r^{max}_{u,MID} = 0.93$.

The iterative procedure ends when the filter $F\left(r^{max}_{u,MID}\right)$ applied to reduce the seismic demand is consistent with the pore pressure ratio computed within the liquefiable layer, that is when:

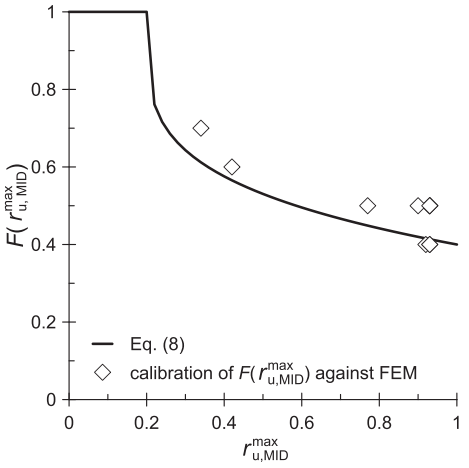


**Fig. 3.** Filter applied to the time histories of shear stress

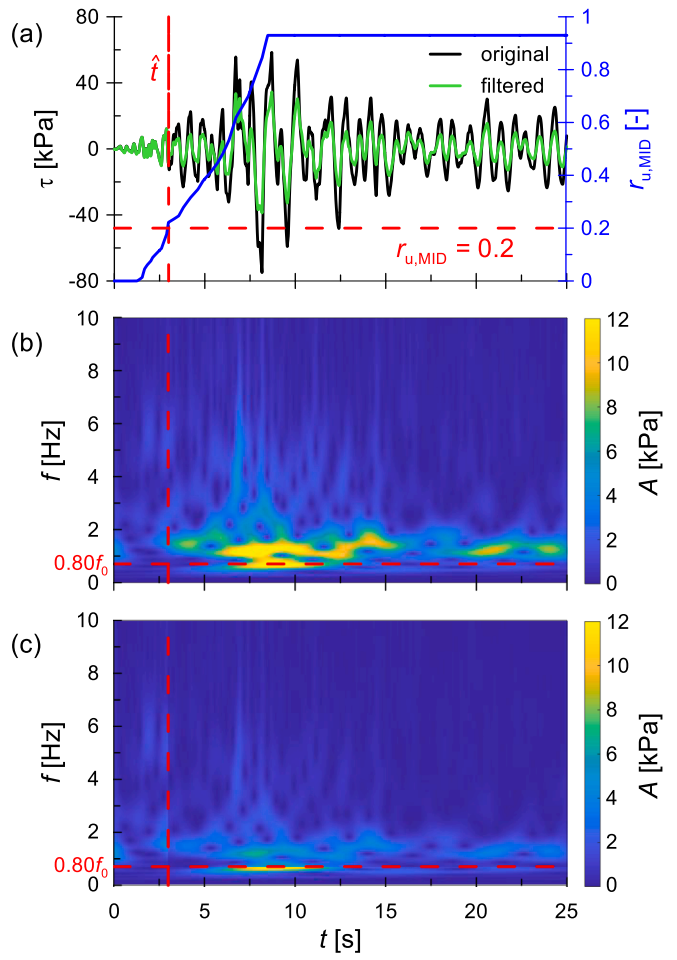


**Fig. 4.** (a) Time histories of the original and filtered shear stress and excess pore pressure ratio; S-transform of the (b) original and (c) filtered shear stress.

$$\left| \frac{r_{u,MID}^{max\ (j)} - r_{u,MID}^{max\ (j-1)}}{r_{u,MID}^{max\ (j-1)}} \right| \leq TOL \tag{11}$$

where $TOL = 1$ % is a prescribed tolerance.

### 2.3. Finite Difference implementation

The proposed method was implemented in a homemade *Matlab* (Mathworks Inc., 2021) routine using the FDM with an explicit Forward-Time, Centered-Space scheme (Recktenwald, 2004). By introducing a uniform discretization of both time and space domain, *i.e.*:

$$\begin{aligned} t_n &= (n-1) \bullet \Delta t, \qquad n = 1, \cdots, (N_t + 1), \qquad N_t = \frac{T_d}{\Delta t} \\ z_i &= (i-1) \bullet \Delta z, \qquad i = 1, \cdots, (N_z + 1), \qquad N_z = \frac{H}{\Delta z} \end{aligned} \tag{12}$$

where $H$ is the total depth of the soil column, Eq. (1) can be easily discretised as:

$$u_i^{n+1} = r_i^n \bullet u_{i+1}^n + \left(1 - 2 \bullet r_i^n\right) u_i^n + r_i^n \bullet u_{i-1}^n + \Delta u_{g,i}^{n+1} \tag{13}$$

where

$$r_i^n = c_{v,i}^n \bullet \frac{\Delta t}{\Delta z^2} \tag{14}$$

and $u_i^{n+1}$ is the unknown excess pore water pressure at time $t = t_{n+1}$ and depth $z = z_i$. The generative term $\Delta u_{g,i}^{n+1}$ is obtained discretising Eq. (2):

$$\Delta u_{g,i}^{n+1} = \frac{\sigma'_{v0,i}}{N_{L,i}} \bullet \chi \bullet \theta \bullet \left(r_{N,i}^{n+1}\right)^{\theta-1} \bullet \left(N_i^{n+1} - N_i^n\right) \tag{15a}$$

where

$$r_{N,i}^{n+1} = r_{N,i}^n + \Delta r_{N,i}^{n+1} = \left(\frac{r_{u,i}^n}{\chi}\right)^{1/\theta} + \frac{\left(N_i^{n+1} - N_i^n\right)}{N_{L,i}} \tag{15b}$$

If $\Delta u_{g,i}^{n+1}$ is set to zero, Eq. (13) describes the evolution of pore pressures both in non-liquefiable layers (during and after shaking) and within the whole soil column throughout the post-shaking reconsolidation phase. It is worth mentioning here that seismic-induced excess pore water pressures can develop also in clayey soil layers, which can be easily considered in the proposed approach by introducing the pertinent excess pore water pressures relation ($r_u$-$r_N$) and cyclic resistance curve (*CSR*-$N_L$) (Zergoun and Vaid, 1994; Boulanger and Idriss, 2006). Nevertheless, here the focus is on the response of liquefiable sandy soils.

Assuming the following initial and boundary conditions:

$$\begin{cases} u|_{(z,t=0)} = 0 \\ u|_{(z=z_w,t)} = 0 \\ \left.\dfrac{\partial u}{\partial z}\right|_{(z=H,t)} = 0 \end{cases} \tag{16}$$

where $z_w$ is the water table depth, and imposing the flow continuity at the boundary between two adjacent layers, Eq. (13) can be solved in time and space, ensuring that the stability condition, $r_i^n < 0.5$, is met.

To account for the effect of pore pressure variations on soil stiffness, the consolidation coefficient at time $t_n$ was computed as function of the current mean effective stress, that is $c_{v,i}^n = k_i E'_{oed}\left(p'^n_i\right)/\gamma_w$. This aspect is crucial for an accurate simulation of the excess pore water redistribution during both the strong motion and the subsequent reconsolidation phase, at least for $r_u$ values larger than 0.5 (Baez and Martin, 1992; Adamidis and Madabhushi, 2016). Quite the opposite, the coefficient of hydraulic conductivity was kept constant over the analysis, as the increase of $k$ with reducing the effective stresses is typically limited compared with the drop of $E'_{oed}$, which results into an overall reduction of $c_v$ when effective stresses reduce (Haigh *et al.*, 2012). Nevertheless, this assumption could be easily overcome by introducing any pertinent function of $k$ with the effective stress or the void ratio (Adamidis and Madabhushi, 2016).

## 3. Validation against coupled FE analyses

The proposed uncoupled Finite Difference (FD) approach was

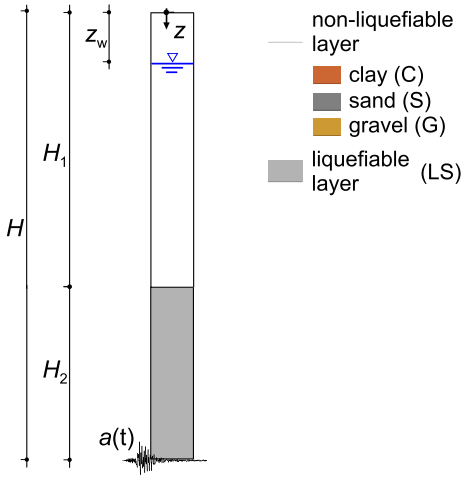


**Fig. 5.** Layout of the stratified 1D soil column.

validated against the results of dynamic coupled FE analyses carried out with Plaxis 2D (Bentley, 2020). Fig. 5 shows the reference layout, consisting of a stratified 1D soil column, with a liquefiable loose sand (LS) overlaid by a non-liquefiable layer, excited by a horizontal acceleration, $a(t)$.

In order to assess the capability of the proposed method to capture the generation and redistribution of excess pore pressures under different conditions, an extensive parametric study was performed, where the geometry of the soil deposit, the hydraulic conductivity of the shallow layer and the seismic input were varied.

As for the geometry, the thickness of the liquefiable layer was changed ($H_2$ = 14, 10 and 5 m) while keeping constant both the total height of the soil column ($H$ = 20 m) and the water table depth ($z_w$ = 5 m). Furthermore, three different values were assumed for the hydraulic conductivity of the non-liquefiable top layer, thus covering a broad range of cases, namely: normally consolidated clay (C), dense sand (S), and gravel (G).

Table 1 summarises the physical and mechanical properties assumed for all soil layers, *i.e.*: saturated soil unit weight, $\gamma_{sat}$; plasticity index, *PI*; minimum, $e_{min}$, and maximum, $e_{max}$, void ratios; void ratio, $e$; relative density, $D_R = (e_{max} - e)/(e_{max} - e_{min})$; friction angle at constant volume (*i.e.*, critical state), $\phi'_{cv}$; at-rest earth pressure coefficient, $k_0 = 1 - \sin\phi'_{cv}$; and hydraulic conductivity, $k$. These parameters are representative of the Vallericca clay (Rampello *et al.*, 1994), Toyoura sand (Verdugo and Ishihara, 1996), and Venado sandstone for the gravel (Seed *et al.*, 1986).

The small-strain shear modulus, $G_0$, was computed according to the empirical equation:

$$\frac{G_0}{p_{ref}} = A \bullet \left(\frac{p'}{p_{ref}}\right)^n \tag{17}$$

where $p_{ref}$ = 100 kPa, while parameters $A$ and $n$ are given in Table 2. Finally, the shear modulus decay, $G/G_0(\gamma)$, and damping, $D(\gamma)$, curves provided by Vucetic and Dobry (1991) for $PI$ = 50 % were adopted for the clay layer, while those by Seed and Idriss (1970) were assumed both for the sand and the gravel.

As shown in Fig. 6, seven seismic inputs were considered in the study, characterised by different amplitude, frequency content and significant duration. Table 3 lists the corresponding ground motion parameters, that is: maximum acceleration, $a_{max}$; dominant, $f_p$, and mean square, $f_{mean}$, frequencies; strong-motion duration, $D_{5\text{-}95}$; Arias intensity, $I_A$; and record duration, $T_{rec}$. The original accelerations were low-pass filtered at 10 Hz and baseline corrected, and a scaling factor *SF* was applied. All cases analysed in the parametric study are reported in Table 4, for a total of 69 analyses. Analyses #43-45 were carried out without applying the signal filtering procedure in the uncoupled approach (Section 2.2.3), to emphasise its influence on the results.

The assumption of an infinitely rigid and impervious bedrock was made in the analyses. Consistently, the seismic inputs were applied at the bottom of the 1D soil column in terms of horizontal acceleration time histories together with a zero-flux hydraulic boundary condition.

In addition to 1D wave propagation analyses, a preliminary set of analyses was also carried out on a 2D Representative Elementary Volume (REV), here intended as a homogeneous soil element with reduced dimensions (0.1 m × 0.1 m), such that it can be considered virtually unaffected by wave propagation effects. The REV was subjected to an irregular shear stress time history, $\tau(t)$, in undrained conditions (Fig. 7). As neither pore-pressure dissipation nor wave propagation can occur in this case, REV analyses allowed validating the assumption of a cumulative distribution of the number of cycles $N(t)$ (Section 2.2.2).

**Table 2**
Parameters adopted to compute the small-strain shear stiffness $G_0$ (Eq. (17)).

| Soil | $A$ – | $n$ – | Reference |
|---|---|---|---|
| clay (C) | 440.50 | 0.837 | Rampello *et al.* (1994) |
| sand (S) | 407.75 | 0.500 | Richart *et al.* (1970) |
| gravel (G) | 834.45 | 0.440 | Nishio *et al.* (1985) |
| liq. sand (LS) | 315.15 | 0.500 | Richart *et al.* (1970) |

### 3.1. Coupled FE analyses

FE analyses were carried out using the standard *u-p* formulation for the equations of the coupled hydro-mechanical problem, with an unconditionally stable implicit time integration scheme. The *SANISAND* constitutive model (Dafalias and Manzari, 2004) was adopted to describe the mechanical behaviour of the liquefiable sand, while the *Hardening Soil model with Small-Strain stiffness* (*HSSmall*; Benz, 2006) was used for the non-liquefiable layers. Tables 5 and 6 summarise the constitutive parameters adopted for the two models, respectively. It is worth mentioning that, for both models, the parameters defining the relationship between the small-strain shear modulus and the mean effective stress were calibrated to reproduce the profile $G_0(p')$ given by Eq. (17) with parameters outlined in Table 2.

Initial geostatic conditions ($\sigma'_{h0}/\sigma'_{v0} = k_0$) were assumed. During the dynamic stage, the horizontal acceleration time history was applied to the bottom nodes of the soil column, together with a zero-water flow condition, thus simulating an infinitely rigid and impervious bedrock. Moreover, impervious and standard periodic constraints were applied along the vertical boundaries to enforce 1D free-field conditions.

In REV analyses, starting from a geostatic stress state characterised by $\sigma'_{v0}$ = 150 kPa and $\sigma'_{h0}$ = 75 kPa, a shear stress time history, $\tau(t)$, was applied to the top nodes, assuming undrained conditions. The base nodes of the REV were fixed, while periodic boundaries were applied along its vertical sides. Specifically, three time histories were applied, all obtained by simply scaling earthquake recordings (N, H and T) to achieve $CSR$ = 0.075 (*i.e.*, $\tau(t) = a(t)/a_{max} \cdot \sigma'_{v0} \cdot CSR/0.65$).

### 3.2. Uncoupled FD analyses

Both the MHD soil model, adopted for the 1D total-stress SSRA, and the $r_u$-$r_N$ and $CSR$-$N_L$ curves, required for the solution of the 1D generation-diffusion model, were calibrated against the results of single element simulations carried out using the *SANISAND* and the *HSSmall* constitutive models, to achieve consistency between the coupled FE and uncoupled FD analyses. With the same purpose, identical boundary conditions (*i.e.*, rigid impervious bedrock) were applied at the base of the 1D soil column.

Parameters $a$, $b$, $c$, and $d$, defining the shear modulus decay and damping curves in the MHD model, were calibrated against the results of strain-controlled drained cyclic shear tests, carried out at $\sigma'_{v0}$ = 150 kPa.

**Table 1**
Physical and mechanical properties of soil layers.

| Soil | $\gamma_{sat}$ kN/m$^3$ | $PI$ % | $e_{min}$ – | $e_{max}$ – | $e$ – | $D_R$ % | $\phi'_{cv}$ ° | $k_0$ – | $k$ m/s |
|---|---|---|---|---|---|---|---|---|---|
| clay (C) | 20 | 50 | – | – | – | – | 23 | 0.609 | $1{\cdot}10^{-6}$ |
| sand (S) | 20 | – | 0.597 | 0.977 | 0.650 | 86.0 | 35 | 0.426 | $5{\cdot}10^{-4}$ |
| gravel (G) | 20 | – | 0.435 | 0.923 | 0.740 | 37.5 | 35 | 0.426 | $1{\cdot}10^{-2}$ |
| liq. sand (LS) | 19 | – | 0.597 | 0.977 | 0.825 | 40.0 | 31 | 0.483 | $5{\cdot}10^{-4}$ |

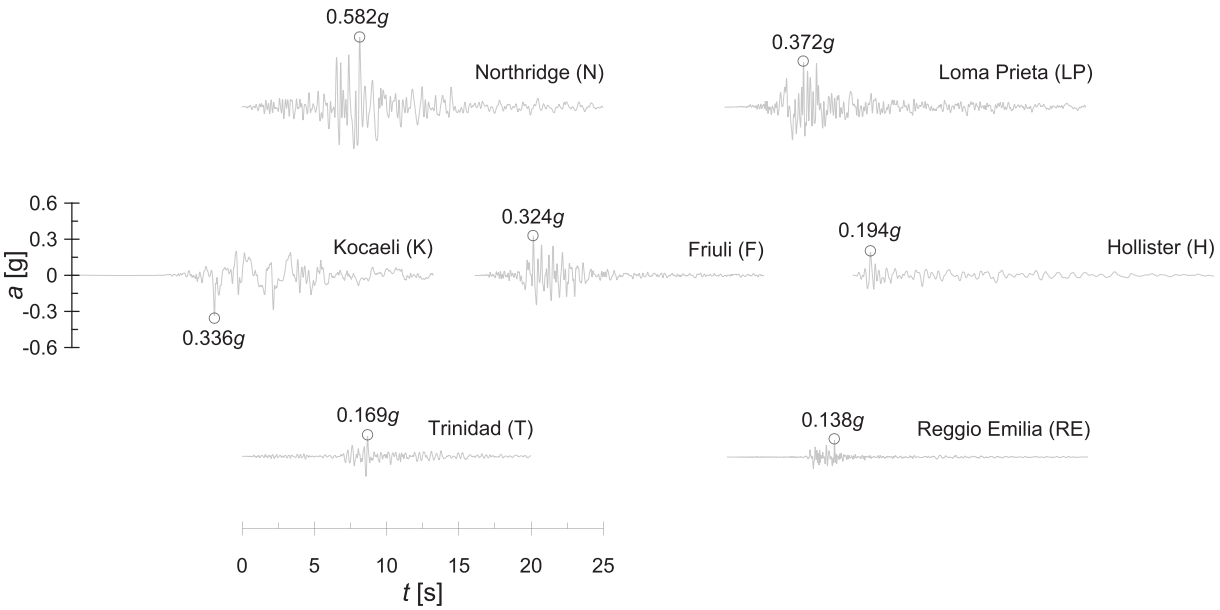


**Fig. 6.** Ground motions adopted in the study.

**Table 3**
Ground motion parameters of the input acceleration time histories.

| Earthquake | $a_{max}$ g | $f_p$ Hz | $f_{mean}$ Hz | $D_{5\text{-}95}$ s | $I_A$ m/s | $T_{rec}$ s |
|---|---|---|---|---|---|---|
| (1994) Northridge (N) | 0.582 | 1.24 | 2.64 | 9.0 | 2.70 | 25 |
| (1989) Loma Prieta (LP) | 0.372 | 0.52 | 3.26 | 10.4 | 1.26 | 25 |
| (1999) Kocaeli (K) | 0.336 | 0.28 | 1.43 | 10.6 | 1.24 | 25 |
| (1976) Friuli (F) | 0.324 | 2.00 | 3.21 | 4.2 | 0.76 | 20 |
| (1961) Hollister (H) | 0.194 | 2.36 | 2.13 | 14.6 | 0.25 | 25 |
| (1983) Trinidad (T) | 0.169 | 2.75 | 3.55 | 7.8 | 0.16 | 20 |
| (1996) Reggio Emilia (RE) | 0.138 | 2.88 | 5.88 | 8.4 | 0.07 | 25 |

Table 7 reports the computed parameters, while Fig. 8 shows a comparison between the reference and computed $G/G_0(\gamma)$ and $D(\gamma)$ curves.

Curves $r_u$-$r_N$ and $CSR$-$N_L$ (Eqs. (3) and (4)) were calibrated against the results of stress-controlled undrained cyclic shear tests, with $CSR$ in the range 0.05-0.25 ($\sigma'_{v0}$ = 150 kPa), representative of the $CSR$ values imposed in the 1D soil column. Fig. 9a shows a comparison between FE results and Eq. (3), the latter computed using both the best-fitting parameters ($\chi = 0.93$, $\theta = 0.84$), and those providing the best agreement with $CSR = 0.075$ ($\chi = 0.89$, $\theta = 1.16$). The first set was used for the analyses of the 1D soil column, while the second one was adopted for the REV analyses, where all the applied inputs were scaled to have the same

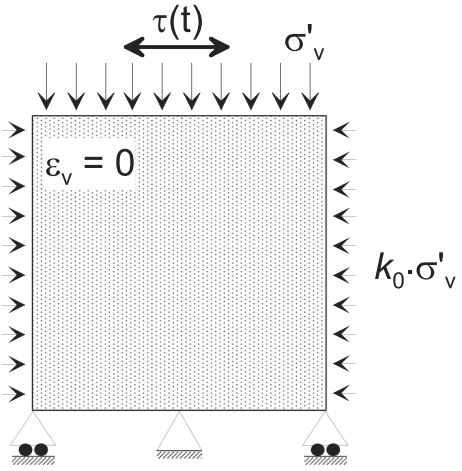


**Fig. 7.** REV layout modelled in the 2D FE analyses.

$CSR$ (= 0.075) value. Finally, a comparison between FE results and Eq. (4) is provided in Fig. 9b, with best-fitting parameters $CSR_t = 0.0195$, $\beta = 0.537$ and $\eta = 1.050$.

**Table 4**
Summary of the analyses carried out in the parametric study.

| Analysis # | Top layer | | Seismic input | $SF$ | $a_{max}$.$SF$ | Filtering in the uncoupled analyses |
|---|---|---|---|---|---|---|
| | Soil | $H_1$ m | | – | g | |
| 1-9 | C, S, G | 15, 10, 6 | N | 1 | 0.582 | yes |
| 10-12 | C, S, G | 10 | LP | 1 | 0.372 | yes |
| 13-21 | C, S, G | 15, 10, 6 | K | 1 | 0.336 | yes |
| 22-30 | C, S, G | 15, 10, 6 | F | 1 | 0.324 | yes |
| 31-33 | C, S, G | 10 | H | 1 | 0.194 | yes |
| 34-42 | C, S, G | 15, 10, 6 | T | 1 | 0.169 | yes |
| 43-45 | C, S, G | 15 | T | 1 | 0.169 | no |
| 46-54 | C, S, G | 15, 10, 6 | K | 0.503 | 0.169 | yes |
| 55-57 | C, S, G | 10 | RE | 1 | 0.138 | yes |
| 58-63 | C, S, G | 15, 10 | F | 0.309 | 0.100 | yes |
| 64-69 | C, S, G | 15, 10 | LP | 0.269 | 0.100 | yes |

**Table 5**
Parameters adopted in the SANISAND constitutive model (liquefiable layer).

| Parameter | Variable | Value |
|---|---|---|
| elasticity | $G_0$ | 125 |
| | $\nu$ | 0.05 |
| critical stateyield surface | $M$ | 1.25 |
| plastic modulus | $c$ | 0.712 |
| | $\lambda_c$ | 0.019 |
| | $e_0$ | 0.934 |
| | $\xi$ | 0.7 |
| yield surface | $m$ | 0.01 |
| | $h_0$ | 7.05 |
| | $c_h$ | 0.968 |
| | $n^b$ | 1.1 |
| dilatancy | $A_0$ | 0.704 |
| | $n^d$ | 3.5 |
| fabric-dilatancy tensor | $z_{max}$ | 4 |
| | $c_z$ | 600 |

### 3.3. Discussion of results

#### 3.3.1. Undrained analyses (REV)

Fig. 10 shows the applied *CSR*(*t*) time histories and the computed excess pore pressures for the scaled Northridge (a), Hollister (b), and Trinidad (c) earthquake, respectively. When considering a cumulative distribution of the equivalent cycles, *N*(t), the results of the simplified approach are in a very good agreement with those provided by coupled FE analyses, both in trend and maximum value. This indicates that the proposed approach describes accurately the progressive accumulation of earthquake-induced excess pore pressures under fully undrained conditions. For comparison, Fig. 10 also displays the results obtained considering a uniform distribution of the equivalent cycles throughout the strong-motion duration. In this case, the method does not describe properly the time evolution of excess pore water pressure.

#### 3.3.2. Partially drained analyses (1D soil column)

Fig. 11 shows a comparison between coupled (FEM) and uncoupled (FDM) approach, for the case of a 1D soil column with $H_1 = 15$ m and $H_2 = 5$ m subjected to the Trinidad (1983) record (Analyses # 34-36 in Table 4). The non-liquefiable shallow layer consists of a clayey (a, d), sandy (b, e) and gravelly (c, f) soil, respectively. Results are shown in terms of time histories of excess pore water pressure ratio, $r_u$, computed at the top and bottom of the liquefiable layer ($z = 15$ and 20 m). Liquefaction was not triggered in all three layouts ($r_u \leq 0.9$), due to the low intensity of the Trinidad input motion (see *e.g.* Table 3). Moreover, as expected, maximum $r_u$ values within the liquefiable sand reduced with increasing the permeability of the overlaying soil layer. An overall

**Table 6**
Parameters adopted in the *HSSmall* constitutive model (non-liquefiable layers).

| Soil | $G_0^{ref}$ MPa | $m$ – | $\gamma_{0.7}$ – | $E_{ur}^{ref}$ MPa | $\nu_{ur}$ – | $E_{50}^{ref}$ MPa | $E_{oed}^{ref}$ MPa | $R_f$ – | $c'$ kPa | $\phi'_{cv}$ ° | $\psi$ ° |
|---|---|---|---|---|---|---|---|---|---|---|---|
| clay (C) | 51.8 | 0.837 | 1.00e-3 | 46.05 | 0.2 | 15.35 | 15.35 | 0.9 | 0 | 23 | 0 |
| sand (S) | 49.1 | 0.500 | 2.40e-4 | 58.90 | 0.2 | 19.65 | 19.65 | 0.9 | 0 | 35 | 0 |
| gravel (G) | 98.2 | 0.440 | 2.40e-4 | 117.85 | 0.2 | 39.30 | 39.30 | 0.9 | 0 | 35 | 0 |

**Table 7**
Soil parameters adopted in the total-stress SSRA (Conti *et al.*, 2020) and in Eqs. (3) and (4) for the comparison of the proposed uncoupled approach against the coupled FE analyses.

| Soil | $a$ – | $b$ – | $c$ – | $d$ – | $\chi$ – | $\theta$ – | $CSR_t$ – | $\beta$ – | $\eta$ – |
|---|---|---|---|---|---|---|---|---|---|
| clay (C) | 0.10 | 10.00 | 0 | 0 | – | – | – | – | – |
| sand (S) | 2.13 | 0.56 | 0 | 0 | – | – | – | – | – |
| gravel (G) | 0.51 | 0.44 | 0 | 0 | – | – | – | – | – |
| liq. sand (LS) | 1.33 | 0.62 | 0.21 | 27.65 | 0.93 | 0.84 | 0.0195 | 0.537 | 1.050 |

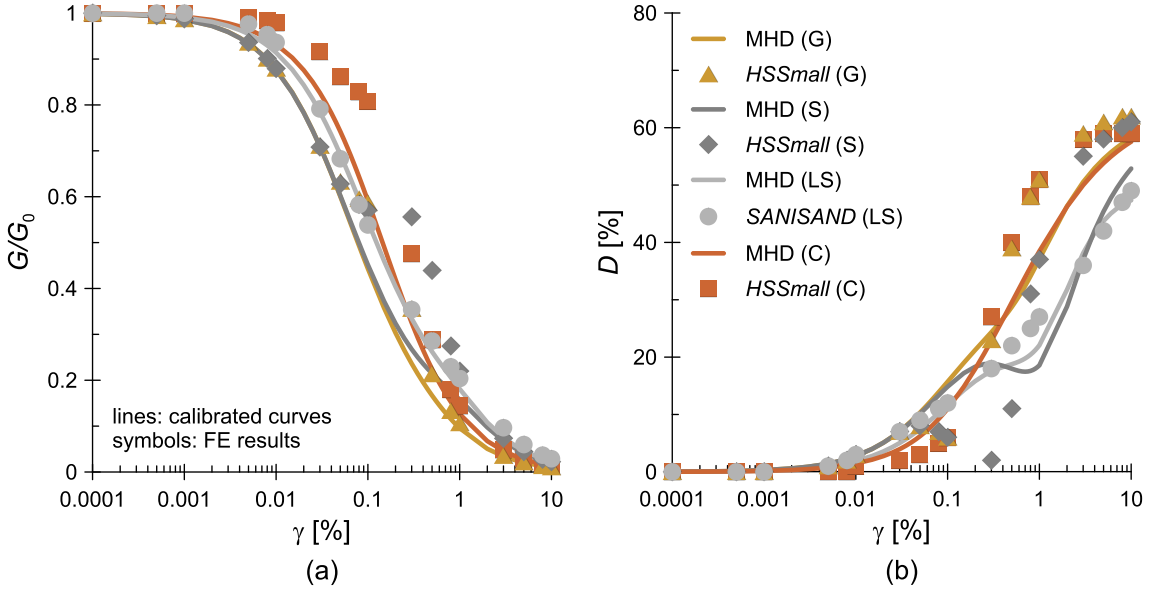


**Fig. 8.** (a) Shear modulus decay curves and (b) damping curves adopted in this study and obtained with simulations of cyclic shear tests in Plaxis *Soil Test.*

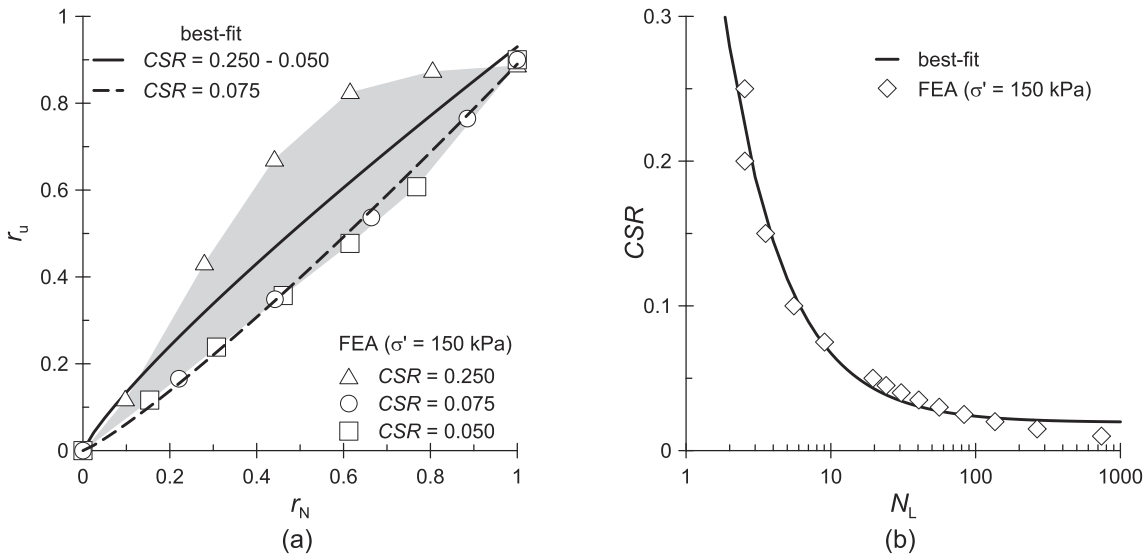


**Fig. 9.** (a) Pore water pressure (Eq. (3)) and (b) cyclic resistance curves (Eq. (4)) adopted in the uncoupled FD computations for comparison with the coupled FE analyses.

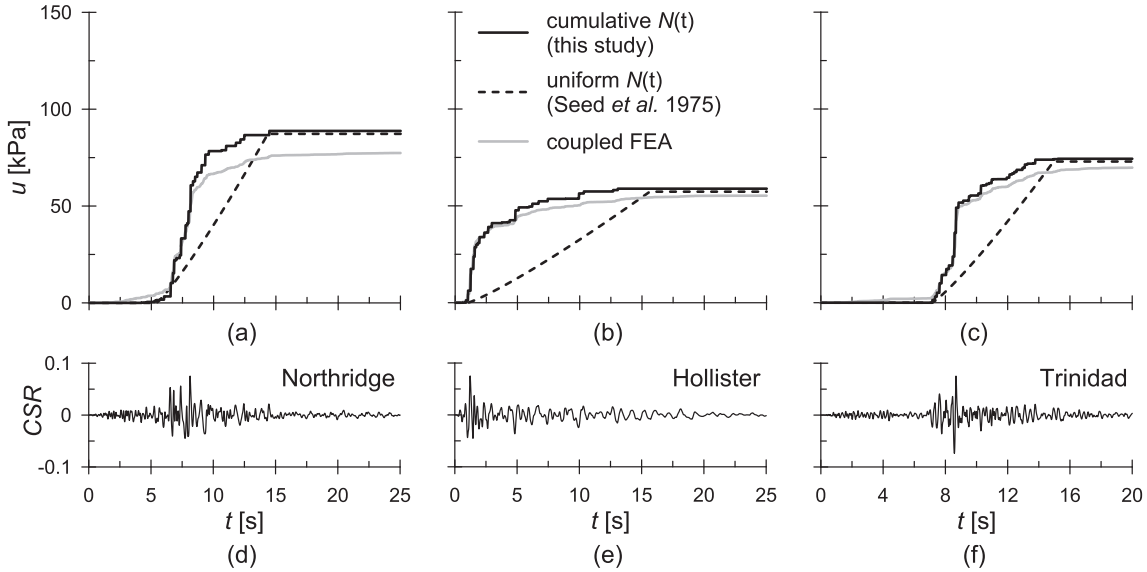


**Fig. 10.** Time histories of the excess pore water pressure obtained from the uncoupled approach and the fully coupled Finite Element Analyses with the REV ((a)–(c)), for three irregular shear stress time histories from different seismic inputs: (d) Northridge, (e) Hollister, and (f) Trinidad.

good agreement is observed between coupled and uncoupled approach, in terms of both maximum value and trend of $r_u$. To highlight the importance of correctly estimating the seismic demand when using an uncoupled approach, Fig. 11 also shows the time history of $r_u$ computed without applying the signal filtering procedure (Section 2.2.3) (Analyses # 43-45). In this case, peak $r_u$ values are typically over twice the FE ones, even bringing to the prediction of complete sand liquefaction in the presence of the top clay layer (Fig. 11a and d). This result is a direct consequence of the overprediction of $N_{eq}$ from the total stress SSRA, as typical in standard uncoupled approaches (Rios *et al.*, 2022).

Fig. 12 shows the space-time contours of $r_u$ for the case of a 1D soil column with $H_1 = H_2 = 10$ m subjected to the Loma Prieta (1989) record (Analyses # 10-12). Results obtained with the proposed uncoupled approach (Fig. 12d–f) are compared with FE ones (Fig. 12a–c), indicating once more a good agreement between the two approaches, in terms of both time and space distribution of $r_u$. In this case, liquefaction was triggered in all layouts, due to the high intensity of the applied earthquake. Nonetheless, the influence of the different hydraulic condition imposed by the shallow layer is still evident. On the one hand, the low-permeability clayey (C) layer inhibits the redistribution and dissipation of excess pore water pressures within the bottom (LS) one, which in turn completely liquefies. On the other hand, the high-permeability gravelly (G) layer imposes a drained boundary to the liquefiable layer, allowing for a quick dissipation of excess pore water pressures right during the strong-motion stage of the earthquake. As expected, in the presence of a shallow dense sand (S) layer, the observed behaviour is halfway between the two cases just discussed.

The overall performance of the proposed method was quantified using an integral parameter, $\delta(z^*)$, defining, for each analysis, the normalised difference between $r_u$ values computed at a specific depth, $z^*$, through the coupled (FE) and uncoupled (FD) approach:

$$\delta(z^*) = \frac{1}{T_{end}} \int_0^{T_{end}} \left| \frac{r_u^{FD}(z^*, t) - r_u^{FE}(z^*, t)}{r_{u,max}^{FE}(z^*)} \right| dt \tag{18}$$

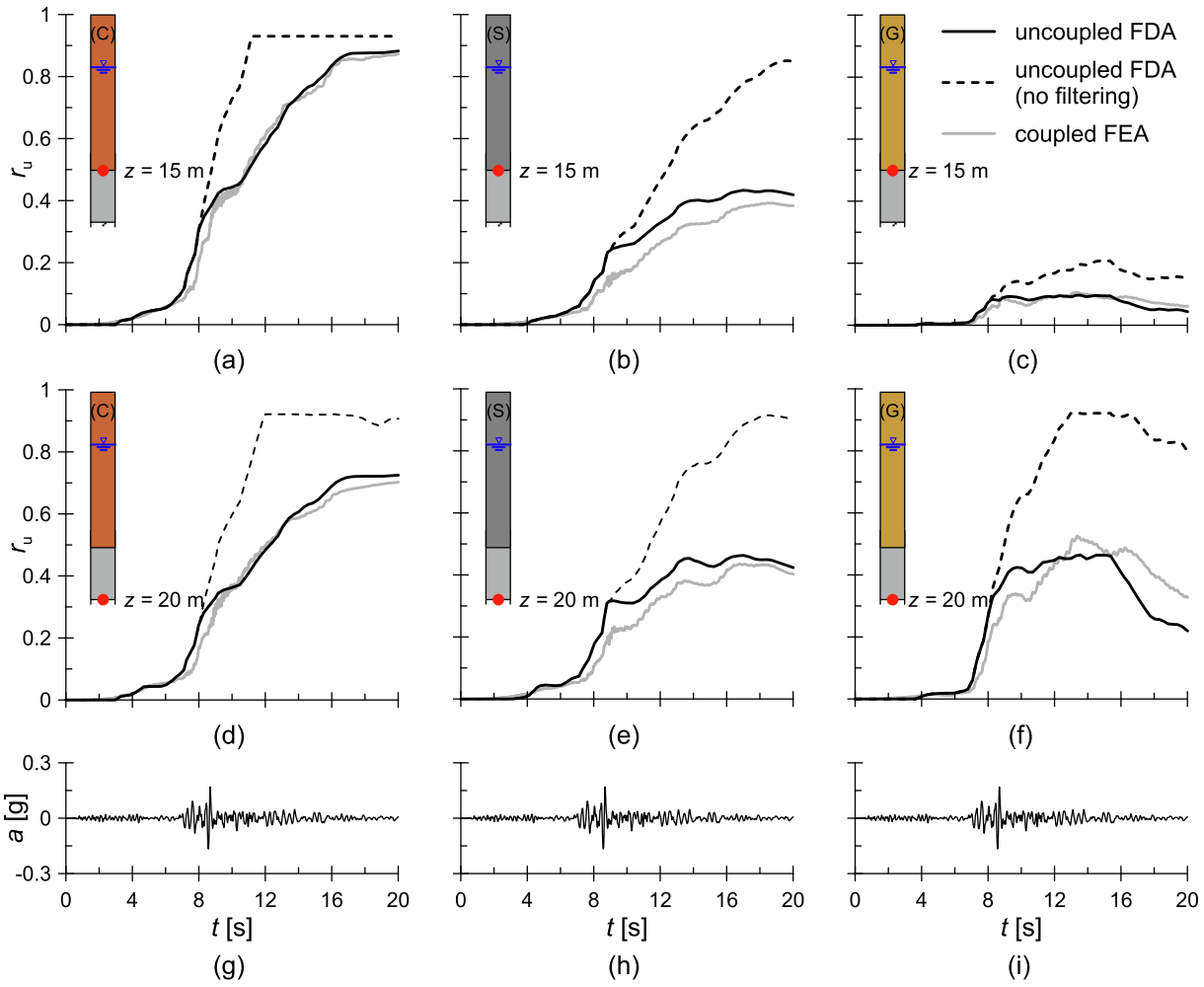


**Fig. 11.** Time histories of the excess pore water pressure ratio from the uncoupled and fully coupled approach for different depths ($z = 15$ m in (a)–(c) and $z = 20$ m in (d)–(f)), different soil configurations (clay in (a), (d); sand in (b), (e) and gravel in (c), (f)) for the Trinidad input motion ((g)–(i)), considering $H_1 = 15$ m and $SF = 1$.

where $T_{end}$ is the total duration of the analysis, here assumed equal to the record duration, $T_{rec}$ (see Table 3); $r_u^{FE}(z^*,t)$ and $r_u^{FD}(z^*,t)$ are the time histories of $r_u$ provided by the FE and FD analyses, respectively, and $r_{u,max}^{FE}(z^*) = \max\left[r_u^{FE}(z^*,t)\right]$. By definition, $\delta(z^*)$ allows to quantify briefly the performance of the uncoupled approach during the whole duration of the applied earthquake, even in the cases when no liquefaction is attained through the soil column. This quantity is plotted in Fig. 13 for all the analyses performed in the parametric study, by taking $z^* = 18$ m as the reference depth. When the filtering procedure is considered, a maximum difference of about 27 % was reached for the soil column subjected to the low intensity Reggio Emilia (RE) record, with a shallow gravel (G) layer. This high value of $\delta(z^*)$ is essentially due to the low intensity of the Reggio Emilia record, which led to a small value of $r_{u,max}^{FE}(z^*) \approx 0.21$, which appears in the denominator of Eq. (18), thus magnifying the resulting $\delta(z^*)$. On average, $\delta(z^* = 18\text{ m}) \approx 9$ %, indicating a good performance of the proposed uncoupled approach. On the contrary, when the filtering procedure is not implemented (Analyses # 43-45), a much larger difference is obtained ($\delta(z^* = 18$ m) up to about 50 %), confirming the need for filtering the seismic demand provided by the total-stress SSRA when using an uncoupled approach.

## 4. Validation against one centrifuge test

The proposed uncoupled approach was also validated against the experimental results of the dynamic centrifuge test M1_GM31, performed by Özcebe *et al.* (2021) as part of the LIQUEFACT project.

### 4.1. Dynamic centrifuge test

Fig. 14a displays the model layout, tested at a centrifugal acceleration of 50*g* and consisting of a homogeneous, 14-m thick layer of saturated, loose Ticino sand TS4 ($D_R$ = 47.5 %), whose physical and mechanical properties are listed in Table 8. Pore water pressures were measured via two alignments of pore pressure transducers (*ppt*), while the applied input motion was recorded through an accelerometer (*acc*) placed at the base of the container. Table 9 summarises the ground motion parameters of the input acceleration.

### 4.2. Uncoupled FD analysis

Model parameters were calibrated against available literature data. Specifically, parameters $A = 996.24$ and $n = 0.42$, defining the small-strain shear modulus profile, $G_0(z)$ (Eq. (17)), were calibrated based on the relation proposed by Fioravante (2000) for Ticino Sand (Fig. 15a). Parameters $a = 0.32$, $b = 0.14$, $c = 0.54$, and $d = 3.44$ for the MHD model were obtained from the best-fit of the $G/G_0(\gamma)$ and $D(\gamma)$ curves proposed by Wichtmann and Triantafyllidis (2013) and Seed and Idriss (1970), respectively (Fig. 15b).

The curve $r_u$-$r_N$ (Eq. (3)) was calibrated against the undrained cyclic

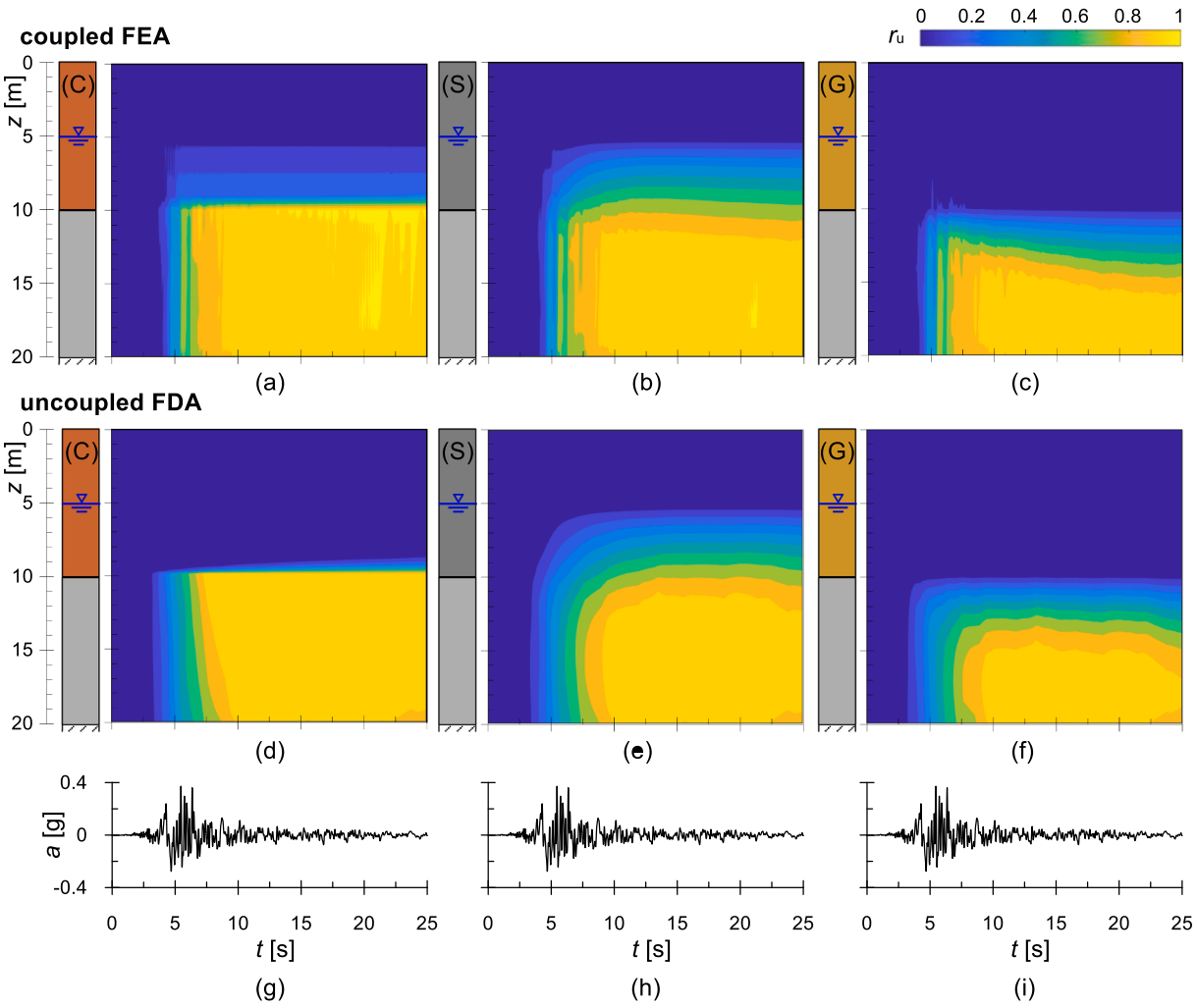


**Fig. 12.** Contours of the excess pore water pressure ratio from the fully coupled ((a)–(c)) and uncoupled ((d)–(f)) approach ($H_1 = 10$ m, $SF = 1$, Loma Prieta input).

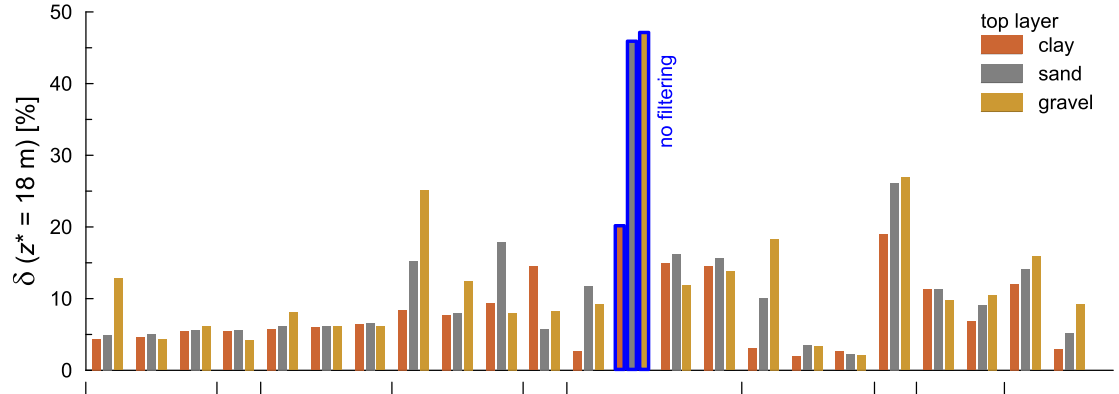


| $H_1$ [m] | 15 | 10 | 6 | 10 | 15 | 10 | 6 | 15 | 10 | 6 | 10 | 15 | 15 | 10 | 6 | 15 | 10 | 6 | 10 | 15 | 10 | 15 | 10 |
|---|---|---|---|---|---|---|---|---|---|---|---|---|---|---|---|---|---|---|---|---|---|---|---|
| input | *N* | | | *LP* | *K* | | | *F* | | | *H* | *T* | | | | *K* | | | *RE* | *F* | | *LP* | |
| *SF* [-] | 1 | | | 1 | 1 | | | 1 | | | 1 | 1 | | | | 0.503 | | | 1 | 0.309 | | 0.269 | |
| $a_{max}$·*SF* [g] | 0.582 | | | 0.372 | 0.336 | | | 0.324 | | | 0.194 | 0.169 | | | | 0.169 | | | 0.138 | 0.100 | | 0.100 | |

**Fig. 13.** Normalised difference between the uncoupled and the coupled analyses, for all cases considered in the parametric study.

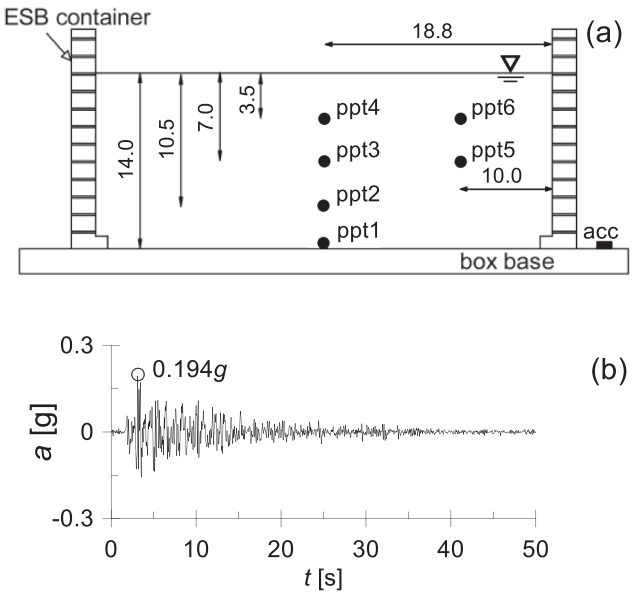


**Fig. 14.** (a) Schematic layout tested in the centrifuge at prototype scale (units: m); (b) input motion (modified from Özcebe *et al.*, 2021).

**Table 8**
Physical and mechanical properties of the Ticino sand (TS4) adopted in the dynamic centrifuge test by Özcebe *et al.* (2021).

| Soil | $\gamma_{sat}$ kN/m$^3$ | $e_{min}$ – | $e_{max}$ – | $e$ – | $D_R$ % | $\varphi'_{cv}$ ° | $k_0$ – | $k$ m/s |
|---|---|---|---|---|---|---|---|---|
| Ticino sand (TS4) | 19.56 | 0.574 | 0.923 | 0.757 | 47.5 | 34.0 | 0.44 | $5\cdot10^{-4}$ |

**Table 9**
Ground motion parameters of the input adopted in the dynamic centrifuge test by Özcebe *et al.* (2021).

| Earthquake | $a_{max}$ g | $f_p$ Hz | $f_{mean}$ Hz | $D_{5-95}$ s | $I_A$ m/s | $T_{end}$ s |
|---|---|---|---|---|---|---|
| GM_31 | 0.194 | 1.06 | 3.23 | 17.75 | 0.58 | 50.0 |

triaxial test by Fioravante and Giretti (2016) for Ticino sand (Fig. 16a), which provided the best-fitting parameters $\chi = 0.90$ and $\theta = 0.55$. Finally, the curve $CSR$-$N_L$ (Eq. (4)) was calibrated against the corresponding numerical curve obtained by Özcebe *et al.* (2021), providing $CSR_t = 0.02$, $\beta = 0.402$ and $\eta = 0.75$.

### 4.3. Discussion of results

Fig. 17 shows the time histories of $r_u$ measured by the *ppts* at four depths within the soil layer, together with those provided by the uncoupled FD analysis. A good comparison is observed at all depths, in terms of both pore pressure build-up and peak values of $r_u$, indicating that the source term $\partial u_g/\partial t$ (Eq. (1)) is properly working at the onset of the strong-motion phase, when concurrent dissipation has a minor effect. As for the consolidation process, the numerical prediction is still in satisfactory agreement with the experimental results, except for the case of *ppt4* and *ppt6*, close to the ground surface ($z = 3.50$ m), where dissipation in the numerical model begins slightly earlier than observed in the centrifuge experiment. Despite the very simplicity of the proposed approach, the overall comparison with centrifuge data can be deemed satisfactory, also considering the saving in computational cost guaranteed by the uncoupled approach with respect to more refined coupled FE analyses.

## 5. Summary and conclusions

Seismic-induced excess pore water pressures developing in liquefiable sandy soils can be assessed through different approaches characterised by different degrees of accuracy. Coupled approaches are the most accurate, but they require time-consuming non-linear dynamic analyses and rely upon advanced constitutive soil models, often difficult to calibrate. Conversely, uncoupled approaches, based on simplifying but physically-sound assumptions, are more suitable for the design practice due to their simplicity, and can be used for the assessment of liquefaction hazard at a large scale. However, as standard uncoupled approaches are developed under fully undrained conditions, they cannot provide any information on the generation and redistribution of earthquake-induced pore water pressures related to the hydraulic interaction between adjacent layers.

In this paper, a novel uncoupled procedure was developed, allowing to model properly the partially drained response of saturated sandy soils during an earthquake. Substantial modifications were introduced with respect to the original approach by Seed *et al.* (1975) to improve the estimation of the pore water pressure build-up, namely: a more realistic

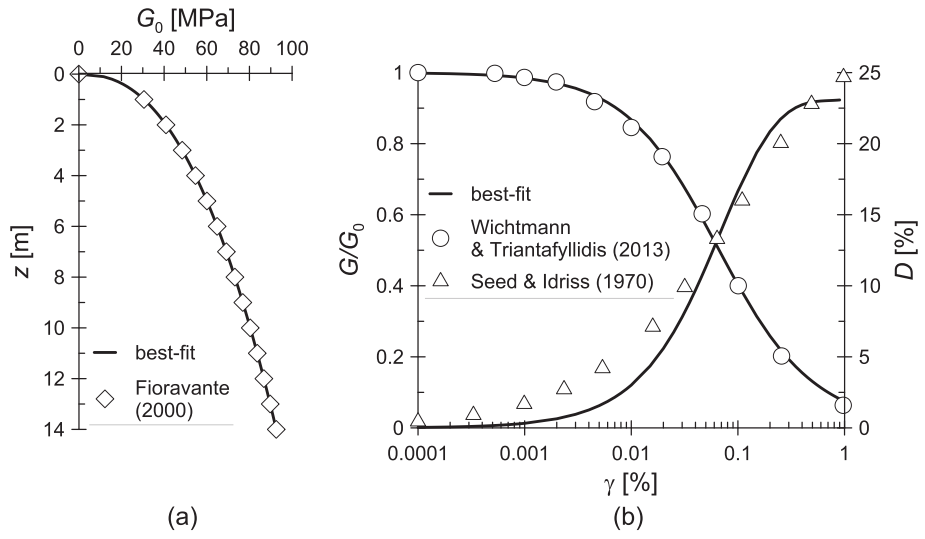


**Fig. 15.** (a) Small-strain shear modulus profile; (b) shear modulus decay and damping curves.

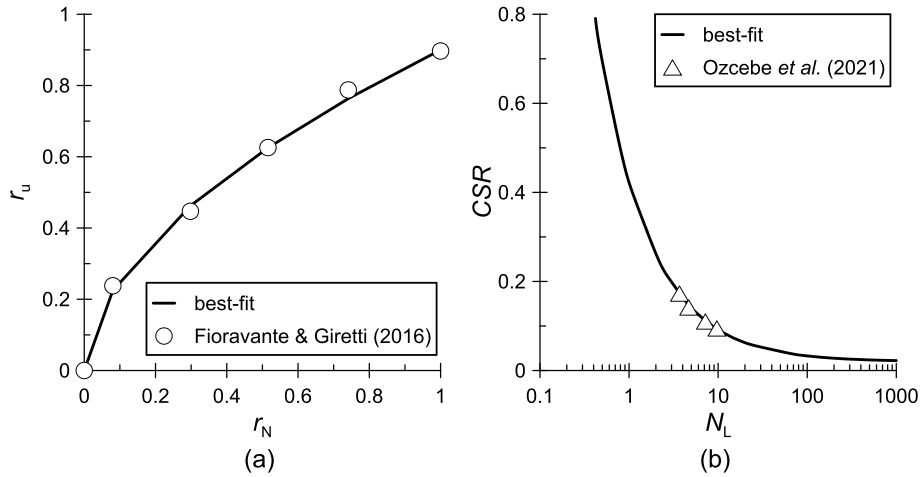


**Fig. 16.** (a) Pore water pressure and (b) cyclic resistance curves adopted in the validation against centrifuge tests.

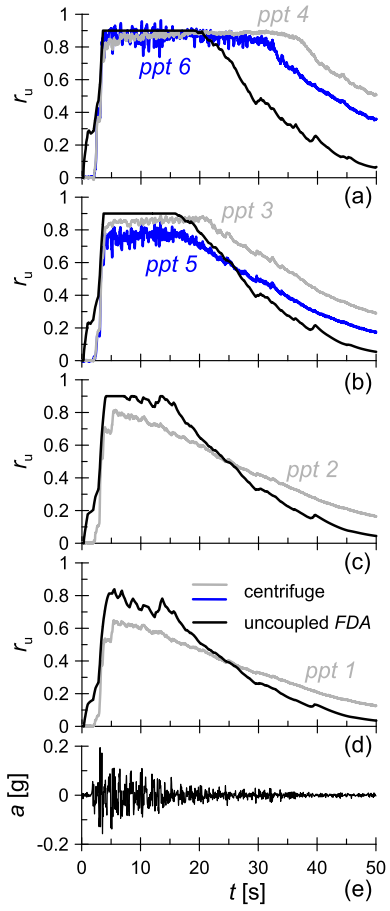


**Fig. 17.** Time histories of the excess pore water pressure ratio from the uncoupled approach and the centrifuge: (a) *ppt4* and *ppt6* ($z = 3.5$ m); (b) *ppt3* and *ppt5* ($z = 7.0$ m); (c) *ppt2* ($z = 10.5$ m); (d) *ppt1* ($z = 14.0$ m); (e) input motion (modified from Özcebe *et al.*, 2021).

non-uniform distribution of equivalent loading cycles; soil stiffness degradation and filtering of shear stresses within the 1D soil column, caused by the pore water pressures build-up occurring in liquefiable layers. All these changes were shown to have a significant impact on the capability of the proposed uncoupled approach to properly predict the timing and amount of earthquake-induced pore water pressures, as well as the subsequent diffusion process.

The proposed approach was implemented in a Matlab routine through the Finite Difference Method and validated against both fully coupled dynamic FE analyses and one experimental centrifuge test. As for the FE analyses, two reference problems were considered. The first problem, where fully undrained conditions were imposed to a REV model, allowed validating the assumption of a cumulative distribution of the number of cycles $N(t)$. The second problem, consisting of a two-layer 1D soil column, allowed assessing the predictive capabilities of the proposed approach in a realistic boundary value problem, where partially drained conditions may affect the generation and diffusion of excess pore water pressures within the liquefiable sand and the adjacent layers. An extensive parametric study was carried out, including different configurations of the 1D soil column, hydraulic conductivity of the shallow layer and seismic inputs, to verify the reliability to the proposed approach. Overall, a good comparison was obtained with both FE analyses and the dynamic centrifuge test, thus confirming that key features of liquefaction were well captured by the uncoupled approach, despite the adopted simplifying assumptions.

Thanks to its generality and ease of implementation, the proposed method can be easily applied to the analysis of a $n$-strata ($n \geq 1$) 1D soil column. As a further strength of the method, it could be extended to axial-symmetric conditions, thus permitting to improve standard uncoupled approaches for the analysis and design of drains to mitigate liquefaction hazard.

## CRediT authorship contribution statement

**Gabriele Boccieri:** Writing – original draft, Validation, Software, Methodology, Investigation, Data curation, Conceptualization. **Domenico Gaudio:** Writing – review & editing, Writing – original draft, Validation, Supervision, Software, Investigation, Conceptualization. **Riccardo Conti:** Writing – review & editing, Supervision, Methodology, Investigation, Funding acquisition, Conceptualization.

## Declaration of competing interest

The authors declare the following financial interests/personal relationships which may be considered as potential competing interests: Gabriele Boccieri reports financial support was provided by Lazio Region. If there are other authors, they declare that they have no known competing financial interests or personal relationships that could have appeared to influence the work reported in this paper.

## Data availability

Some or all data that support the findings of this study are available

from the corresponding author upon reasonable request.

## Acknowledgments

This project was supported by Regione Lazio's programme POR-FSE 2014-2020 under grant agreement no. F85F21001280003. Numerical FE analyses were performed thanks to the support by Bentley and Dr. Sandro Brasile.

## References

Adamidis, O., Anastasopoulos, I., 2022. Cyclic liquefaction resistance of sand under a constant inflow rate. Géotechnique 1–14.
Adamidis, O., Madabhushi, S.P.G., 2016. Post-liquefaction reconsolidation of sand. Proc. R. Soc. A: Math. Phys. Eng. Sci. 472 (2186), 20150745.
Baez, J.I., Martin, G.R., 1992. Quantitative evaluation of stone column techniques for earthquake liquefaction. In: Earthq Eng. 10th World Conf, pp. 1477–1483.
Bentley, 2020. Plaxis 2D CE v20 – Reference Manual. Delft University of Technology, Delft, The Netherlands.
Benz, T., 2006. Small-Strain Stiffness of Soils and its Numerical Consequences. University of Stuttgart (Ph.D. thesis).
Bouckovalas, G.D., Tsiapas, Y.Z., Theocharis, A.I., Chaloulos, Y.K., 2016. Ground response at liquefied sites: seismic isolation or amplification? Soil Dyn. Earthq. Eng. 91, 329–339.
Boulanger, R.W., Idriss, I.M., 2014. CPT and SPT based liquefaction triggering procedures. Report No. UCD/CGM.-14(1).
Boulanger, R.W., Idriss, I.M., 2006. Liquefaction susceptibility criteria for silts and clays. J. Geotech. Geoenv. Eng. ASCE 132 (11), 1413–1426.
Chiaradonna, A., Flora, A., 2020. On the estimate of seismically induced pore-water pressure increments before liquefaction. Géotech. Lett. 10 (2), 128–134.
Chiaradonna, A., Tropeano, G., d'Onofrio, A., Silvestri, F., 2018. Development of a simplified model for pore water pressure build-up induced by cyclic loading. Bull. Earthq. Eng. 16 (9), 3627–3652.
Chiaradonna, A., Lirer, S., Flora, A., 2020. A liquefaction potential integral index based on pore pressure build-up. Eng. Geol. 272, 105620 https://doi.org/10.1016/j.enggeo.2020.105620.
Conti, R., Angelini, M., Licata, V., 2020. Nonlinearity and strength in 1D site response analyses: a simple constitutive approach. Bull. Earthq. Eng. 18, 4629–4657. https://doi.org/10.1007/s10518-020-00873-5.
Cubrinovski, M., Ntritsos, N., 2023. 8th Ishihara lecture: Holistic evaluation of liquefaction response. Soil Dyn. Earthq. Eng. 168, 107777.
Cubrinovski, M., Rhodes, A., Ntritsos, N., Van Ballegooy, S., 2019. System response of liquefiable deposits. Soil Dyn. Earthq. Eng. 124, 212–229.
Dafalias, Y.F., Manzari, M.T., 2004. Simple plasticity sand model accounting for fabric change effects. J. Eng. Mech. 130 (6), 622–634.
Fioravante, V., 2000. Anisotropy of small strain stiffness of Ticino and Kenya sands from seismic wave propagation measured in triaxial testing. Soils Found. 40 (4), 129–142.
Fioravante, V., Giretti, D., 2016. Unidirectional cyclic resistance of Ticino and Toyoura sands from centrifuge cone penetration tests. Acta Geotech. 11 (4), 953–968.
Haigh, S.K., Eadington, J., Madabhushi, S.P.G., 2012. Permeability and stiffness of sands at very low effective stresses. Géotechnique 62 (1), 69–75.
Hancock, J., Bommer, J.J., 2005. The effective number of cycles of earthquake ground motion. Earthq. Eng. Struct. Dyn. 34 (6), 637–664.
Khashila, M., Hussien, M.N., Karray, M., Chekired, M., 2018. Use of pore pressure build-up as damage metric in computation of equivalent number of uniform strain cycles. Canad. Geotech. J. 55 (4), 538–550.
Kramer, S.L., Sideras, S.S., Greenfield, M.W., 2016. The timing of liquefaction and its utility in liquefaction hazard evaluation. Soil Dyn. Earthq. Eng. 91, 133–146.
Mathworks Inc., 2021. Matlab version 9.10.0 (R2021a). Natick, Massachusetts.
Millen, M.D., Viana da Fonseca, A., Azeredo, C.M., 2021. Time–frequency filter for computation of surface acceleration for liquefiable sites: equivalent linear stockwell analysis method. J. Geotech. Geoenv. Eng. 147 (8), 04021070.
Minaka, U.S., Okamura, M., Ono, K., 2021. Verification of effectiveness and design procedure of gravel drains for liquefaction remediation. Soils Found. 61, 1191–1206.
Miner, M.A., 1945. Cumulative damage in fatigue. Trans. ASME 67, A159–A164.
Ni, M., Abdoun, T., Dobry, R., El-Sekelly, W., 2021. Effect of field drainage on seismic pore pressure buildup and Kσ under high overburden pressure. J. Geotech. Geoenv. Eng. 147 (9), 04021088.
Nishio, N., Tamaoki, K., Machida, Y., 1985. Dynamic deformation characteristics of crushed gravel by means of large-size triaxial test apparatus. In: Proc. 20th Ann. Conv., Japan. Soc. Soil Mech. Found. Eng., Tokyo, Japan. pp. 603–604.
Ntritsos, N., Cubrinovski, M., 2024. Ground-motion effects on liquefaction response. Soil Dyn. Earthq. Eng. 177, 108392.
Özcebe, A.G., Giretti, D., Bozzoni, F., Fioravante, V., Lai, C.G., 2021. Centrifuge and numerical modelling of earthquake-induced soil liquefaction under free-field conditions and by considering soil–structure interaction. Bull. Earthq. Eng. 19 (1), 47–75.
Özener, P.T., Greenfield, M.W., Sideras, S.S., Kramer, S.L., 2020. Identification of time of liquefaction triggering. Soil Dyn. Earthq. Eng. 128, 105895.
Park, T., Park, D., Ahn, J.K., 2015. Pore pressure model based on accumulated stress. Bull. Earthq. Eng. 13 (7), 1913–1926.
Ramirez, J., Barrero, A.R., Chen, L., Dashti, S., Ghofrani, A., Taiebat, M., Arduino, P., 2018. Site response in a layered liquefiable deposit: evaluation of different numerical tools and methodologies with centrifuge experimental results. J. Geotech. Geoenv. Eng. 144 (10), 04018073.
Rampello, S., Viggiani, G.M.B., Silvestri, F., 1994. The dependence of small strain stiffness on stress state and history for fine grained soils: the example of Vallericca clay. Int. Symp. Pre-Failure Def. Charact. Geomat. 273–278.
Recktenwald, G.W., 2004. Finite-difference approximations to the heat equation. Mech. Eng. 10 (1), 1–27.
Richart, F.E., Hall, J.R., Woods, R.D., 1970. Vibrations of Soils and Foundations. Prentice-Hall Inc.
Rios, S., Millen, M., Quintero, J., da Fonseca, A.V., 2022. Analysis of simplified time of liquefaction triggering methods by laboratory tests, physical modelling and numerical analysis. Soil Dyn. Earthq. Eng. 157, 107261.
Seed, H.B., Idriss, I.M., 1970. Soil moduli and damping factors for dynamic response analyses. Report No. EERC 70-10, Earthq. Eng. Research Centre, University of California, Berkeley, California.
Seed, H.B., Idriss, I.M., 1971. Simplified procedure for evaluating soil liquefaction potential. J. Soil Mech. Found. Div. ASCE 97 (SM9), 1249–1273.
Seed, H.B., Martin, P.P., Lysmer, J., 1975. The Generation and Dissipation of Pore Water Pressures During Soil Liquefaction. University of California, College of Engineering.
Seed, H.B., Wong, R.T., Idriss, I.M., Tokimatsu, K., 1986. Moduli and damping factors for dynamic analyses of cohesionless soils. J. Geotech. Eng. 112 (11), 1016–1032.
Sinha, S.K., Ziotopoulou, K., Kutter, B.L., 2024. Effects of Excess Pore Pressure Redistribution in Liquefiable Layers. J. Geotech. Geoenv. Eng. ASCE 150 (4), 04024014.
Stockwell, R.G., Mansinha, L., Lowe, R.P., 1996. Localization of the complex spectrum: the S transform. IEEE Trans. Signal Process. 44 (4), 998–1001.
Terzaghi, K., 1923. Die Berechnung der Durchassigkeitsziffer des Tones aus dem Verlauf der hydrodynamischen Spannungs. erscheinungen. Sitzungsber. Akad. Wiss. Math. Naturwiss. Kl. Abt. 2A 132, 105–124.
Tropeano, G., Chiaradonna, A., d'Onofrio, A., Silvestri, F., 2019. A numerical model for non-linear coupled analysis of the seismic response of liquefiable soils. Comp. Geotech. 105, 211–227.
Verdugo, R., Ishihara, K., 1996. The steady state of sandy soils. Soils Found. 36 (2), 81–91.
Vucetic, M., Dobry, R., 1991. Effect of soil plasticity on cyclic response. J. Geotech. Eng. 117 (1), 89–107.
Wichtmann, T., Triantafyllidis, T., 2013. Effect of uniformity coefficient on G/Gmax and damping ratio of uniform to well-graded quartz sands. J. Geotech. Geoenv. Eng. 139 (1), 59–72.
Zergoun, M., Vaid, Y.P., 1994. Effective stress response of clay to undrained cyclic loading. Canad. Geotech. J. 31 (5), 714–727.